

A method for effective beam widths of slabs in flat plate structures under gravity and lateral loads

Jung-Wook Choi†

Department of Civil & Environmental Engineering, University of Alberta, 3-059 Markin/CNRL Natural Resources Engineering Facility, Edmonton AB T6G 2W2, Canada

Jin-Gyu Song‡

Division of Architecture, Chonnam National University, 300 Yong-Bong Dong 500-757 Gwangju, Korea

(Received January 3, 2005, Accepted October 6, 2005)

Abstract. Effective beam width models are commonly used to obtain the lateral stiffness of flat plate structures. In these models, an effective beam width is defined as the width when the flexural stiffness of the beam element equals the slab stiffness. In this present study, a method to obtain effective beam widths that considers the effects of connection geometry and slab cracking is analytically proposed. The rectangularity of the vertical member for the connection geometry and the combined effects of creep and shrinkage for the slab cracking are considered. The results from the proposed method are compared with experimental results from a test structure having nine slab-column connections.

Key words: effective beam width; elastic width; stiffness reduction; connection geometry; slab cracking; reinforced concrete; flat plate structure.

1. Introduction

In effective beam width models, an actual slab is replaced with a beam element, which rotates uniformly across its transverse width. The beam element has a thickness equal to that of the slab, and an effective beam width that is defined by matching the flexural stiffness of the beam element to that of the slab. The two most common techniques for modeling a slab-column system as a frame are shown in Fig. 1 (Hwang and Moehle 1993, 2000, Grossman 1997).

Many analytical and experimental studies for obtaining the effective beam width have been performed. Some studies focused on defining the elastic widths of the effective beam according to connection geometries. Others concerned the stiffness reduction phenomenon due to cracking in the analysis model. Each study was based on the elastic and non-elastic behavior of the slab. However, previous studies for obtaining the effective beam width have not been concerned enough with the effect of vertical member rectangularity in connection geometries and the combined effects of creep

† Ph.D., Post-Doc

‡ Associate Professor, Corresponding author, E-mail: jgsong@chonnam.ac.kr

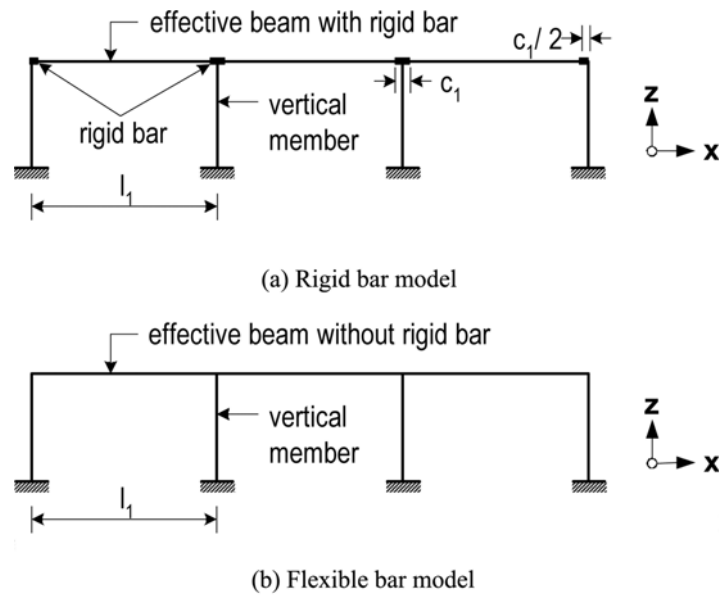


Fig. 1 Effective beam width model

and shrinkage in stiffness reduction.

This paper proposes a method for obtaining more accurate values of effective beam widths in design. To achieve this objective, the following studies were conducted.

- 1) A parametric study to obtain the elastic widths of the effective beams was performed by using a finite element technique. This study considers the rectangularity of the vertical member.
- 2) A study of the reduction in lateral stiffness due to slab cracking was conducted. The effect of the service gravity loads and the combined effects of creep and shrinkage were considered.
- 3) A test structure with two bays in each direction and nine columns was tested laterally and analyzed by using the finite element technique. The results obtained from the proposed elastic widths and stiffness reduction factors are compared to the analytical and experimental results.

2. Elastic effective beam width

2.1 General description of the elastic width

Many analytical techniques for obtaining elastic effective beam widths (l_e) have been proposed. A common approach for these techniques is to cut a typical interior connection under lateral load only from a continuous floor system and then to bound the connection by lines of inflection and symmetry as shown in Fig. 2. These lines are assumed to be located along the slab mid-spans perpendicular and parallel to the loading direction. Actually, the position of the inflection lines will change if the stiffness of adjacent vertical members located parallel to the loading direction is not the same. However, this change is generally ignored to simplify a study.

A joint region exists wherever the slab connects to a vertical member. The total flexural stiffness of the connection increases with the stiffness of the joint region. As shown in Fig. 3, Aalami (1972)

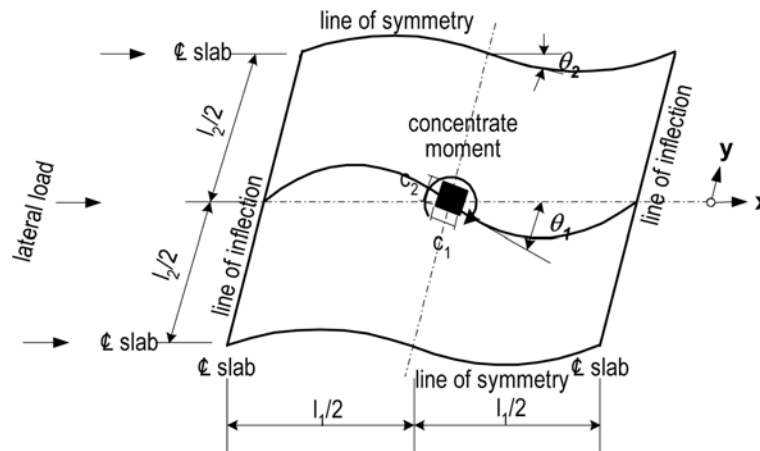


Fig. 2 A slab-vertical member connection

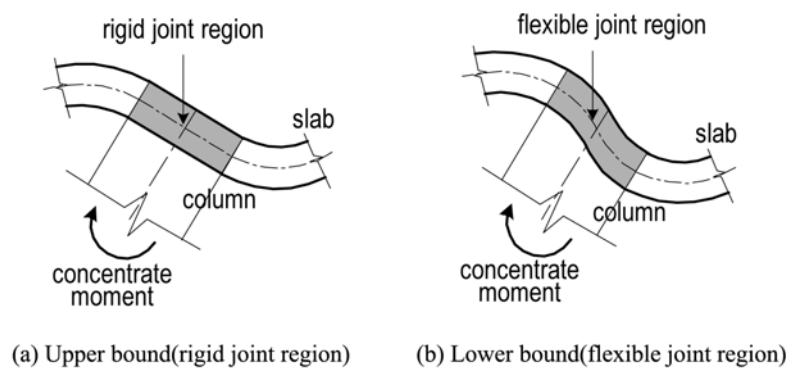


Fig. 3 Two bounds on the stiffness of the joint region

assumed two bounds on the stiffness of the joint region: one considers the slab within the joint region to be rigid; the other assigns a joint flexibility equal to that of the surrounding slab. The behavior of the joint region depends on the relative flexural stiffness between the joint region and the surrounding slab. In most practical cases, this relative stiffness is high, so most analytical investigations have idealized the joint region as rigid (Pecknold 1975). Based on this assumption, an elastic stiffness value for a connection can be obtained.

Although the rigid joint assumption is selected for an elastic stiffness value, the elastic widths of the effective beam in the two models shown in Fig. 1 should be defined differently according to the joint modeling techniques. For a simple evaluation between the elastic width of the two models, Hwang and Moehle (2000) proposed the factor of $1/(1 - c_1/l_1)^3$.

2.2 Parametric study for interior connections

An elastic effective beam width (l_e) represents the elastic stiffness of a slab connected to a vertical member. The elastic stiffness of the slabs is affected by connection geometries. To obtain the elastic widths, slabs with different geometric conditions are modeled by using the finite element technique,

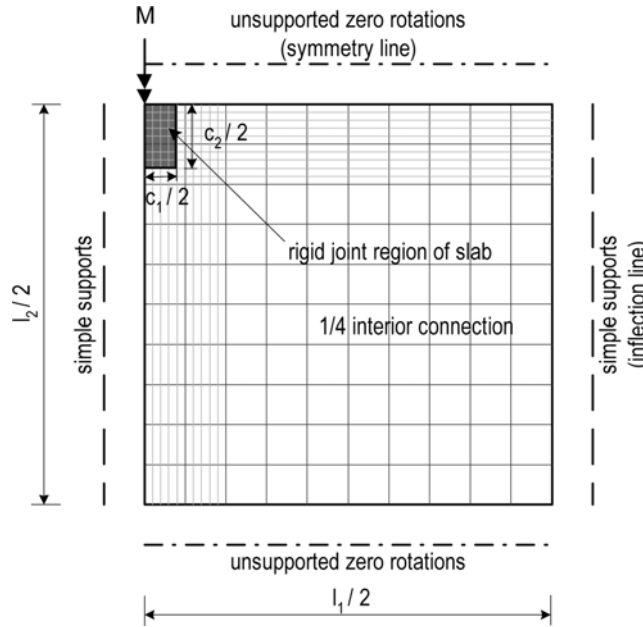
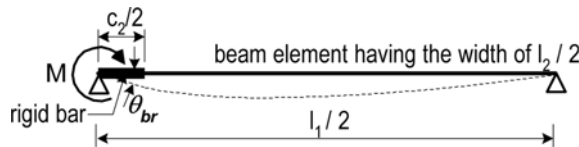
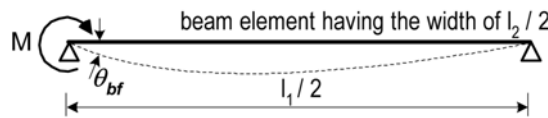


Fig. 4 Finite element model



(a) Rigid bar model



(b) Flexible bar model

Fig. 5 Beam element analysis

as shown in Fig. 4. In the finite element model, applied loads transferred from a vertical member to a slab are represented by using the concentrated moment load (M) applied at the center of the joint region, which is treated rigidly. Structural analyses are performed by using a general purpose software named MIDAS-GEN (2003), and then with the results of the analyses, the slab rotations (θ_s) at the center of the joint region are acquired. The slab's flexible stiffness can be calculated by using M/θ_s .

The stiffness of the beam elements for rigid and flexible bar models can be obtained by dividing the moment load (M) by the beam rotations (θ_{br} and θ_{bf}), as shown in Fig. 5. The elastic widths for both models can be calculated by equating the flexural stiffness of the beam element to that of the slab.

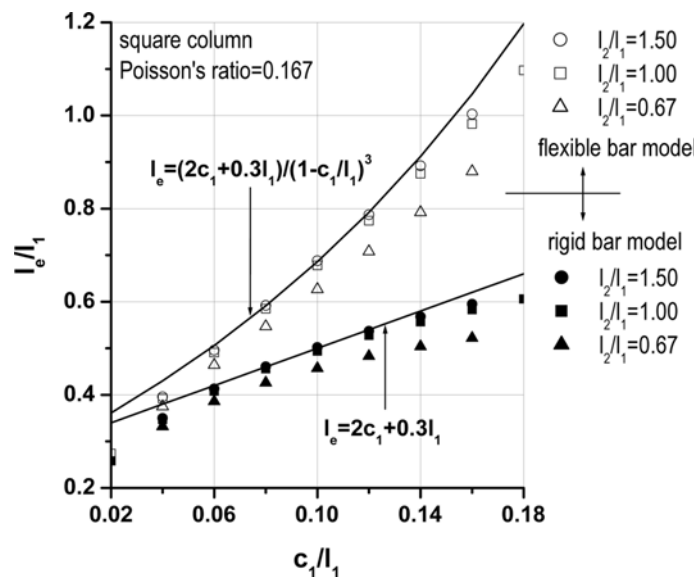


Fig. 6 Elastic widths for different values of the c_1/l_1 and l_2/l_1 ratios for rigid & flexible bar models

Fig. 6 shows the elastic widths of the interior connections with square vertical members. The range of the geometric parameters was $0.02 \leq c_1/l_1 \leq 0.18$ and $0.67 \leq l_2/l_1 \leq 1.5$. The elastic widths rapidly increase with an increase in c_1/l_1 . By comparison, the slab aspect ratio has little effect on the elastic width when l_2/l_1 is greater than 1. When $l_2/l_1 < 1$, the elastic widths decrease with a decrease of the ratio l_2/l_1 . These results are similar to the findings reported by Pecknold (1975). The trend of the results for the rigid bar model can be approximated by the function $l_e = 2c_1 + 0.3l_1$, which slightly overestimates the elastic stiffness of the connections within the range of $l_2/l_1 \leq 1$. The adjustment factor of $1/(1 - c_1/l_1)^3$ for the flexible bar model matches well with the finite element solutions.

With respect to the rectangularity of the vertical member, Pecknold (1975) reported that a variation of the c_2/c_1 ratio from 1/2 to 2 changed the elastic width less than 2 percent. Allen and Darvall (1977) studied the influence of c_2 for a range of values of c_2/l_1 from 0.03 to 0.12 and found its effect to be negligible. Based on these findings, Hwang and Moehle (2000) did not consider the rectangularity of the vertical member in their study of elastic widths. In the present study, variations on the elastic width of about 16% for the rigid bar model and 22% for the flexible bar model were found within the range of c_2/c_1 from 0.5 to 2.0 (when c_1/l_1 of the square slab was equal to 0.1). The considerable discrepancy between the previous and present studies may arise from differences in the modeling techniques relative to the slab and the joint region.

To study the effect of vertical member rectangularity, the ratio of c_2/l is increased in the finite element model with a square flat slab from 0.04 to 1. Fig. 7 shows the elastic widths for different values of c_2/l in both models. The elastic widths in the rigid bar model approach the slab width as c_2/l increases. This finding shows that a slab acts as an ordinary beam element; thus, the upper bound of the elastic widths in the rigid bar model should be limited to the slab transverse width. The function $l_e = 2c_1 + 0.3l_1 + 0.8(c_2 - c_1)$ models the effect of the vertical member rectangularity on elastic widths within the range of c_2/l 0.04~1 and c_2/c_1 0.5~2. In Fig. 7(b), some of the values for the elastic width of the flexible bar model exceed the slab transverse width

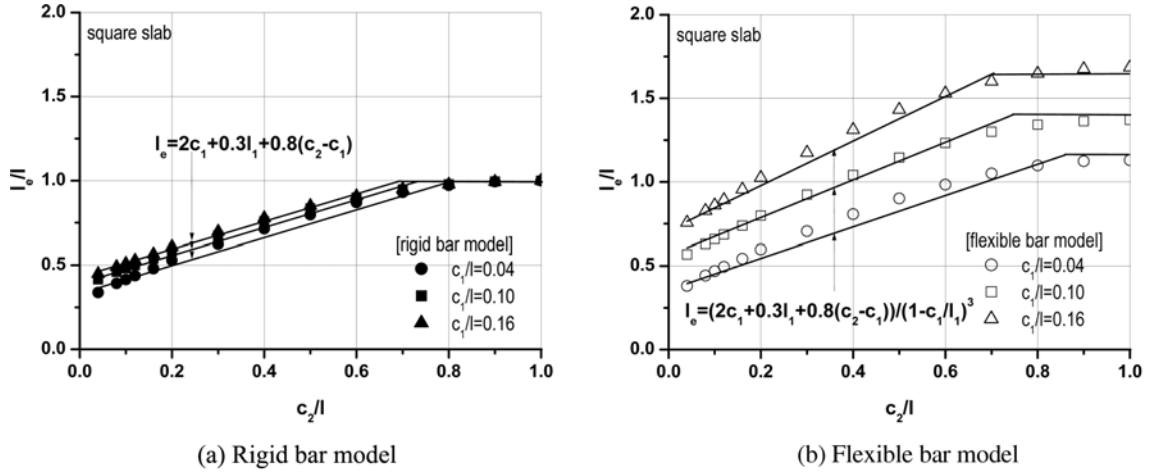


Fig. 7 Elastic widths for different values of the c_1/l ratios

because the stiffening effect due to rigid body behavior of the joint region in the slab is reflected on the elastic widths of the beam elements in the flexible bar model.

2.3 Implementation in design practice

A flat plate structure includes two distinct substructures, the interior frame and the exterior frame, as shown in Fig. 8. For the connections in an interior frame, the elastic effective beam widths for a rigid bar model can be represented as

$$l_e = 2c_1 + 0.3l_1 + 0.8(c_2 - c_1), \quad l_e \leq l_2 \tag{1}$$

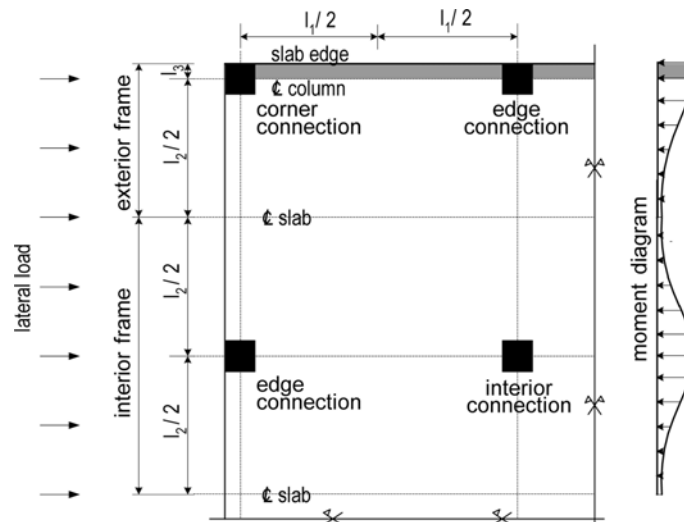


Fig. 8 Flat plate structures

Although Eq. (1) is based on a study of interior connections, it can be applied to edge connections in an interior frame because of the similarity of the lateral behavior between both connections. Hwang and Moehle (2000) and Grossman (1997) adopted a similar approach.

For an exterior frame, some adjustment of Eq. (1) is required. As shown in Fig. 8, the dimension l_3 is the distance from the slab edge to the centerline of the vertical member. The slab rotation of the strip in the dimension l_3 is assumed to be equal to the uniform rotation of the effective beam element. Thus, the elastic widths for the exterior frame can be calculated as the sum of half of the values obtained from Eq. (1) and l_3 :

$$l_e = c_1 + 0.15l_1 + 0.4(c_2 - c_1) + l_3, \quad l_e \leq l_2/2 + l_3 \quad (2)$$

Eq. (2) would be used where the slab edge is flush with the outside face of the vertical member. In the case of a slab with an overhang, Eq. (2) can overestimate the actual stiffness of the slab in an exterior frame but this kind of slab is not considered in the present study.

The values obtained from Eqs. (1) and (2) are applicable to the rigid bar model, where rigid bars having the length of $c_1/2$ model the joint region at both ends of the beam element. If the rigid bars are not included in the model, the widths given by Eqs. (1) and (2) should be multiplied by the factor of $1/(1 - c_1/l_1)^3$.

3. Effective beam width with stiffness reductions (l_2')

3.1 Stiffness reduction phenomenon

A reduction in lateral stiffness due to slab cracking has been reported (Hwang and Moehle 2000, Pan and Moehle 1992, Moehle and Diebold 1984, Robertson and Durrani 1992, 1991). To reflect this phenomenon in lateral load analysis, a stiffness reduction factor β (the ratio of the reduced non-linear stiffness to its elastic value) has often been proposed. Moehle and Diebold (1984) suggested a factor between 1/2 and 1/3 for elastic effective beam widths. ACI 318-02 (2002) recommended a factor of 1/4 for a lower bound value to evaluate the effects of cracking on stiffness.

The flexural stiffness of slabs is reduced due to slab cracking caused from not only externally applied gravity loads but also internal creep and shrinkage effects. The reduced flexural stiffness directly affects the lateral stiffness of flat plate frames.

Different stiffness reduction phenomena occur during the service life of a concrete slab:

- 1) Immediate stiffness reduction due to the effect of service gravity loads (β_s).
- 2) Additional stiffness reduction due to the combined effects of creep and shrinkage (β_l).

3.2 The effect of service gravity loads (β_s)

For slabs under service gravity loads, the stiffness values based on Eq. (3) can be used:

$$I_e = \left(\frac{M_{cr}}{M_a}\right)^3 I_g + \left[1 - \left(\frac{M_{cr}}{M_a}\right)^3\right] I_{cr} \quad (3)$$

Eq. (3) accounts for the immediate stiffness reduction due to the gravity load and can be rearranged to provide an expression for β_s :

$$\beta_s = \frac{I_e}{I_g} = \left(\frac{M_{cr}}{M_a}\right)^3 + \left[1 - \left(\frac{M_{cr}}{M_a}\right)^3\right] \frac{I_{cr}}{I_g} \quad (4)$$

However, computations of the M_a , M_{cr} , I_g , and I_{cr} are not convenient. A simplified method to calculate β_s is preferred.

Using Eq. (4), a parametric study for β_s is performed. In this study, the parameters are defined by the concrete compression strength (f_{ck}), the length of the clear span in the direction parallel to the lateral load (l_n), and the super-imposed load (L_{SUP}), which is the sum of the super-imposed dead and service live loads. The ratio of the design thickness (h) of a slab to its minimum value (h_{min}) is also included as a parameter. The value of h_{min} is based on the minimum specified in ACI 318-02 (2002) Section 9.5.3.2. The procedure to obtain β_s is as follows:

- (1) The length of the clear span (l_n) from 4 m to 8 m, and the concrete compression strength (f_{ck}) from 20.6 MN/m² to 33.3 MN/m² are chosen.
- (2) The minimum thickness of the interior flat plate slab (h_{min}), fixed at $l_n/33$ in this study, is calculated. The slabs in flat plate structures are generally designed to be thicker than this minimum value. Thus, the effects of slab thickness are represented by the ratio of h/h_{min} , ranging from 1.0 to 1.2.
- (3) Service loads, including the self-weight of the concrete slabs and the super-imposed load, are applied externally. In service loads, the self-weight (normal weight concrete) is calculated by using the designed thickness, and the range of the super-imposed load (L_{SUP}) is set from 1.96 kN/m² to 7.84 kN/m².
- (4) The cracking moment (M_{cr}) for normal weight concrete and the moments of inertia of the gross and cracked concrete section (I_g and I_{cr}) are calculated according to ACI 318-02 (2002) Section 9.5.2.3. The maximum service load moment (M_a) of the interior slabs is obtained by using the Direct Design Method.
- (5) For each unique combination of M_a , M_{cr} , I_{cr} , and I_g , the corresponding value of β_s predicted by Eq. (4) is calculated.

Fig. 9 shows the results from the parametric study of β_s . As shown in Fig. 9(a), l_n has a significant effect on stiffness reduction. With an increase in the l_n , the flexural stiffness of the slabs is very rapidly reduced. This trend is well approximated by the function $f(l_n) = 4.25/l_n$.

The effects of L_{SUP} and f_{ck} are shown in Figs. 9(b) and (c). The flexural stiffness of a slab decreases with an increase in L_{SUP} or a decrease in f_{ck} . The effects of L_{SUP} and f_{ck} are expressed as $f(L_{SUP}) = 0.004/L_{SUP}$ and $f(f_{ck}) = f_{ck}/27$.

Fig. 9(d) displays the variation of β_s values on h/h_{min} . The flexural stiffness is increased with increasing h/h_{min} . The effect of h/h_{min} is approximated by using the function of $f(h/h_{min}) = (h/(1.1h_{min}))^3$.

By multiplying each function, the values for β_s can be calculated:

$$\beta_s = \frac{4.25}{l_n} \times \frac{0.004}{L_{SUP}} \times \frac{f_{ck}}{27} \times \left(\frac{h}{1.1h_{min}}\right)^3, \quad \left(\text{where, } h_{min} = \frac{l_n}{33}\right)$$

$$\beta_s = \frac{17f_{ck}h^3}{L_{SUP}l_n^4} \leq 1 \quad (5)$$

In Eq. (5), every quantity concerning length must be expressed in meters, and β_s is conceptually limited to 1.

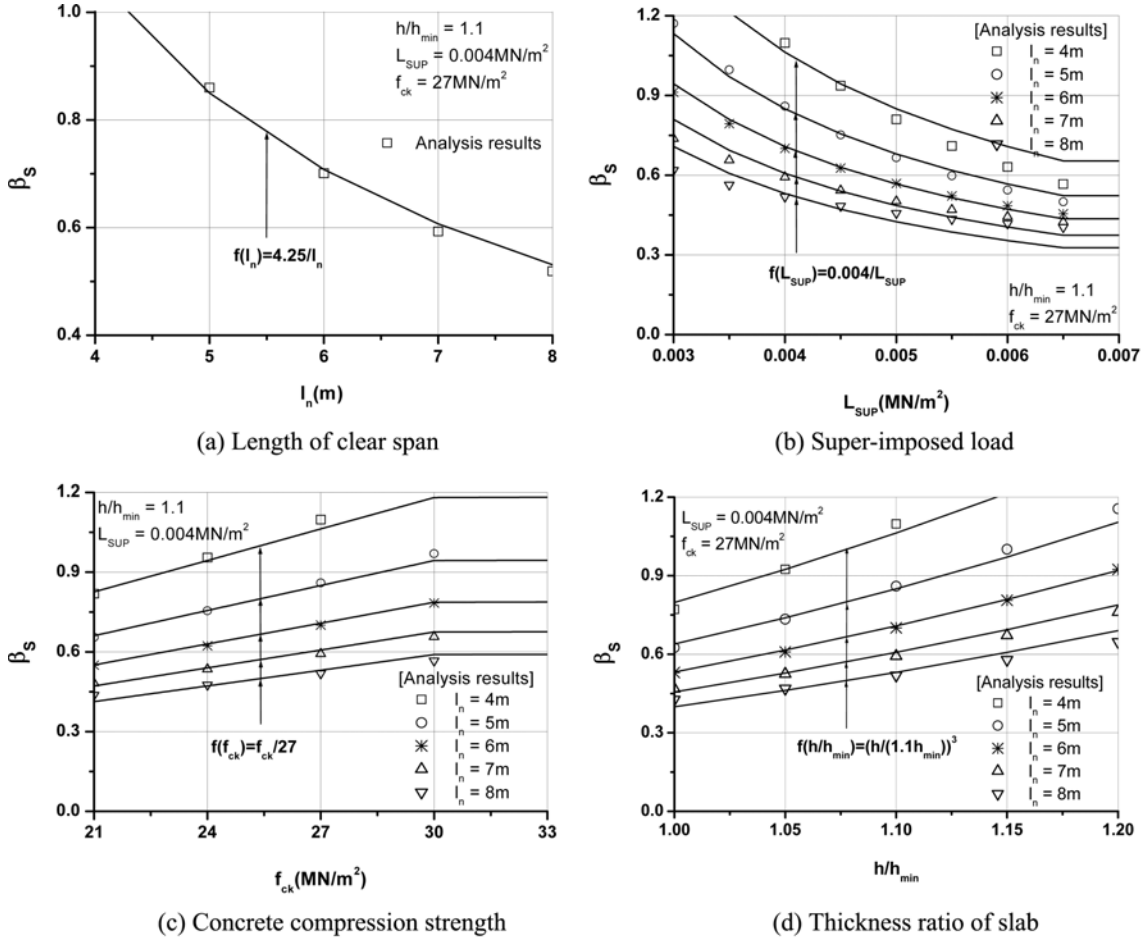


Fig. 9 Parametric study for the stiffness reduction factor (β_s)

3.3 The combined effects of creep and shrinkage (β_L)

Over time, creep and shrinkage strains increase the deflection and the curvature in a flexural member, increasing the crack opening. In a two-way slab, the crack opening cannot develop without an increase in the length of the crack, and this increase results in an increase of concrete cracking and the reduction in the flexural stiffness of the slab.

For stiffness reduction due to creep and shrinkage effects, Eq. (6) can be used if we assume that the flexural stiffness of members is inversely proportional to its deflection (ACI 318-02 2002):

$$\delta_{CP+SH} = \frac{\xi}{1 + 50\rho'} \times \delta_{SUS} \quad (6)$$

In Eq. (6), the multiplier ξ is the time-dependent factor used to calculate additional long-term deflection resulting from creep and shrinkage. This multiplier ranges between 0 and 2 depending on the time period. The ratio ρ' accounts for the effect of compression reinforcement in reducing additional long-term deflection. However, the bottom reinforcement of the slab near the vertical

member may not be compressed under gravity loads. Thus, $50\rho'$ can be ignored:

$$\delta_{CP+SH} = \xi \delta_{SUS} \quad (7)$$

Based on elastic behavior assumption, the sustained load deflections (δ_{SUS}) in Eq. (7) can be expressed as a proportional relation of the immediate deflections (δ_{DL+LL}) due to service gravity loads. Thus, additional long-term deflections of Eq. (7) can be modified as

$$\delta_{CP+SH} = \xi \frac{L_{SUS}}{DL + LL} \delta_{DL+LL} \quad (8)$$

A final deflection is computed as the sum of the immediate and additional long-term deflections ($\delta_{DL+LL} + \delta_{CP+SH}$):

$$\delta_{FL} = \frac{\xi L_{SUS} + DL + LL}{DL + LL} \delta_{DL+LL} \quad (9)$$

By considering the inversely proportional relationship between the deflection and flexural stiffness of a member, the final flexural stiffness at the stage of computing the final deflection can be expressed by

$$EI_{FL} = \frac{DL + LL}{\xi L_{SUS} + DL + LL} EI_{DL+LL} \quad (10)$$

From Eq. (10), the combined effects of creep and shrinkage for stiffness reduction are extracted as

$$\beta_L = \frac{DL + LL}{\xi L_{SUS} + DL + LL} \quad (11)$$

In Eq. (10), EI_{DL+LL} is the stiffness reduced by the effect of service gravity loads and thus is equal to the elastic stiffness (EI_g) multiplied by β_S . Therefore, Eq. (10) can be rewritten by

$$EI_{FL} = \beta_L \beta_S EI_g \quad (12)$$

The stiffness reduction due to service gravity loads and the combined effects of creep and shrinkage can be defined by

$$\beta_L \times \beta_S = \frac{DL + LL}{\xi L_{SUS} + DL + LL} \times \frac{17f_{ck}h^3}{L_{SUP}l_n^4} \geq \frac{1}{4} \quad (13)$$

The lower limit of 1/4 in Eq. (13) is consistent with ACI 318-02 (2002) and is based on the assumption of a fully cracked slab with minimum reinforcement at all locations.

4. Evaluation of the proposed effective beam width model

A flat plate structure with nine slab-column connections was tested under lateral loads and analyzed by using the finite element technique. Based on the lateral stiffness of the structure obtained from the test and FE analysis, the effective beam width model proposed in this study was evaluated.

4.1 Lateral load test of the structure with nine slab-column connections

The prototype is a flat plate structure typical of a multi-story apartment building. The test structure was constructed at half scale and consisted of four $2.75 \text{ m} \times 1.65 \text{ m}$ rectangular panels and nine 250 mm square columns protruding 0.7 m above and below the slab as shown in Fig. 10. The slab thickness was 90 mm.

The prototype slab was designed in accordance with ACI 318-02 (2002). The design service gravity load consisted of 4.21 kN/m^2 self-weight of the slab and 1.96 kN/m^2 super-imposed dead load. The design service live load was 2.94 kN/m^2 . Yield strength of 392 MN/m^2 for the flexural reinforcement and a compressive strength of 26.5 MN/m^2 for the concrete slab were assumed. The actual properties of the material at the time of testing are tabulated in Table 1. The equivalent frame method was used to calculate gravity load moments. The total unbalanced moment resulting from a lateral load consistent with a moderate earthquake was obtained by using the effective beam width model proposed in this paper. In the test structure, the slab was reinforced with 10 mm diameter (cross-sectional area of 71 mm^2) bars; the column was reinforced with eight 16 mm diameter (cross-sectional area of 199 mm^2) longitudinal bars and 10 mm diameter ties. Fig. 11 shows the layout of the top and bottom slab reinforcement.

The elevation and photo views of the overall test set-up are shown in Fig. 12. The lower end of the column representing the mid-height of the story was designed to act as a pinned support. The top of the column was connected to a loading frame, which distributed equal lateral displacement to the columns, by means of the pinned-pinned connector with a load cell. The test was performed at

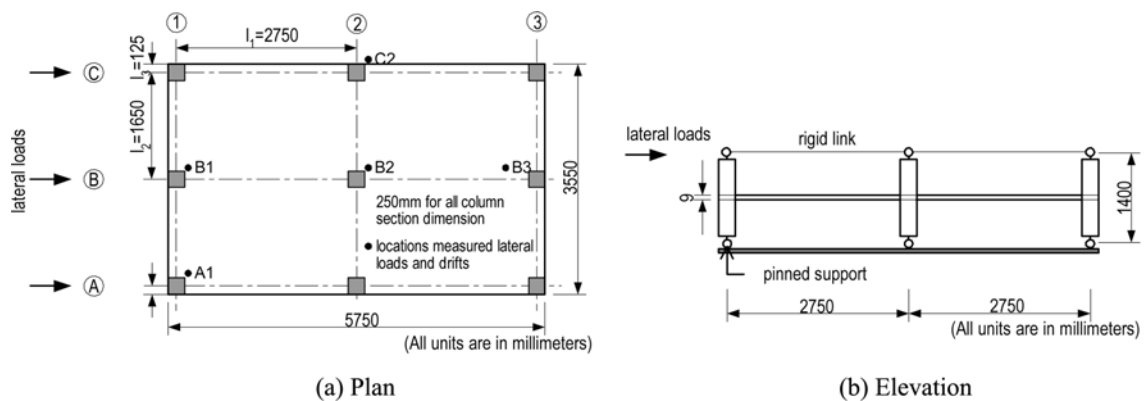


Fig. 10 Half scale test structure

Table 1 Material properties

Member	Concrete properties (MN/m^2)		Reinforcing bars properties (MN/m^2)			
	Compressive strength f'_c	Modulus of elasticity E_c	Bar size	Yield strength f_y	Ultimate strength f_u	Modulus of elasticity E_s
Slab	27.2	22295	10M	383	502	203154
Column			16M	432	570	212954

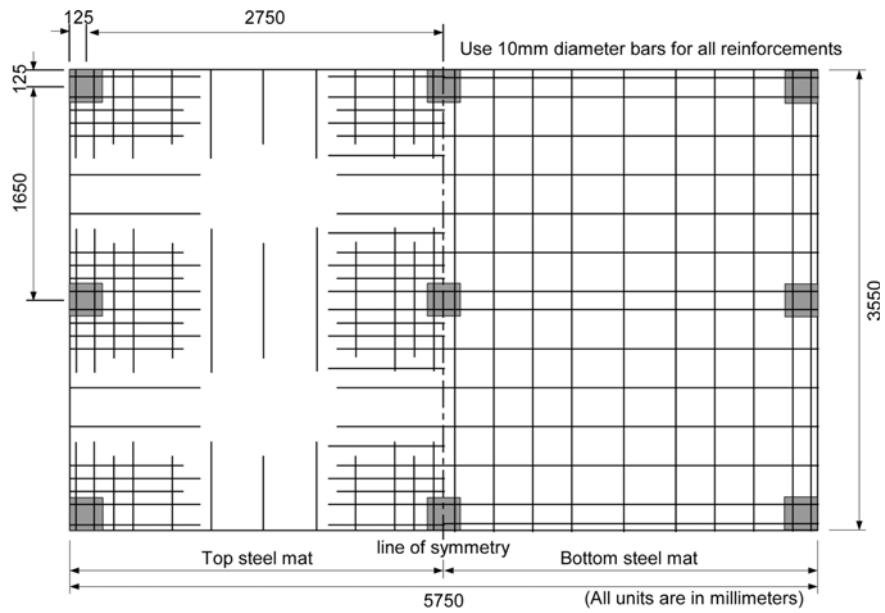
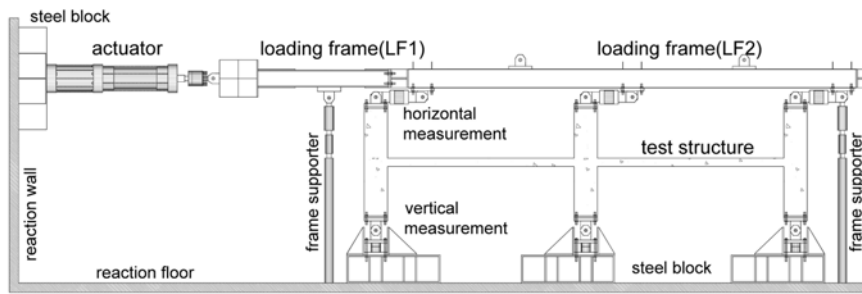


Fig. 11 Layout of the slab reinforcement



(a) Setup elevation in the long direction



(b) View photograph

Fig. 12 Test setup

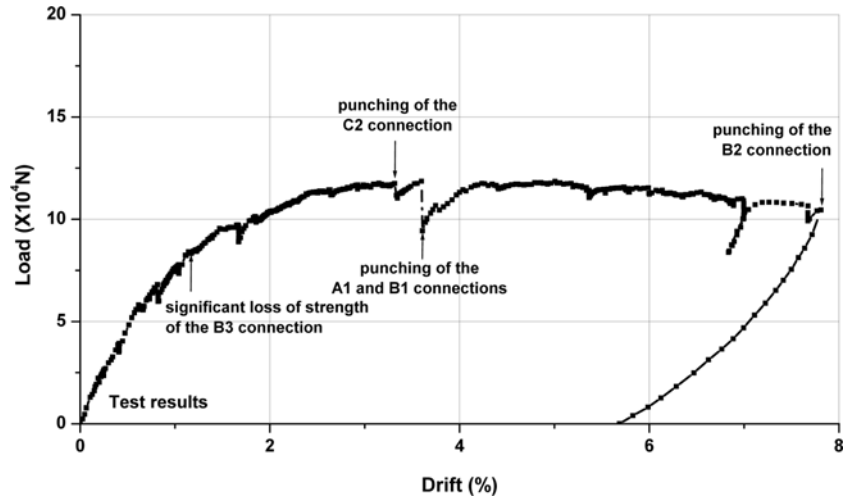


Fig. 13 Overall load-deflection relation of the test structure

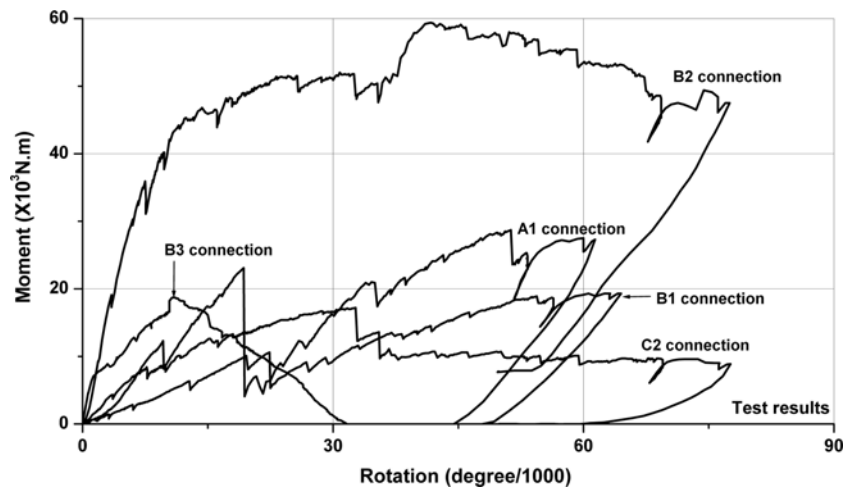


Fig. 14 Moment-rotation relations of the selected connections

around three months after casting. The test structure was vertically loaded with weights on top of the concrete slab to simulate service gravity loads. The total applied vertical load was approximately 7 kN/m^2 , which included the service load, the super-imposed dead load, and half the self-weight of the prototype slab to compensate for the reduced self-weight of the test slab. Finally, the lateral displacement load was applied in the long direction of the test structure.

The lateral load-deflection relation obtained from the experiment is shown in Fig. 13, and the moment-rotation relations for the selected connections (A1, B1, B2, B3, and C2 shown in Fig. 10) are shown in Fig. 14. Lateral loads were measured by the load cell connected to the actuator and the top of the column. Lateral drifts were determined from lateral drift readings at the top ends of the column. The moment of the each connection was calculated by multiplying the lateral loads measured at the top of the column by the interstory height. The rotation of the each connection was

obtained by dividing the lateral drifts measured at the top ends of the column by the interstory height.

The overall load-deflection relation of the test structure indicates progressive degradation in stiffness with increasing drift. The significant loss of strength in the test occurred to the connection B3 at a drift of 1.15%, but a sudden decrease in the overall strength of the test structure did not occur. The connection C2 was punched at a drift of 3.32%, and then the connections A1 and B1 were punched at a drift of 3.6%. After a sudden drop in strength at a drift of 3.6%, A1 and B1 connections in the test structure were re-strengthened with an increase in the rotation as shown in Fig. 14. The test structure finally failed to sustain the lateral load with the punching shear failure of the interior connection B2 at a drift of 7.8%. The lateral load-deflection relation shown in Fig. 13 demonstrates the test structure's excellent drift capacity.

4.2 Analytical lateral stiffness of the test structure

The elastic stiffness of the test structure was obtained numerically by using the finite element model shown in Fig. 15. The slab was modeled by 560 four-node quadrilateral plate elements by using the linear analysis program MIDAS-GEN. The reinforcement was not modeled. Poisson's ratio was taken to be equal to $1/6$. The plates in joint regions were made effectively rigid, having a stiffness six orders of magnitude greater than the plates outside the joints. The finite element model was then linearly analyzed.

The test structure was also modeled by using two effective beam width models: one for the elastic widths (l_e) and one for the effective beam widths with stiffness reductions (l'_2). For the both effective beam width models, the beams were modeled to span with rigid end zones from the center line to the face of the column. The top ends of all the columns were connected by a rigid link to enforce equal lateral displacements.

The elastic widths for individual connections of the prototype structure were first calculated by using Eqs. (1) and (2), and the elastic widths for the spans between the adjacent connections were taken as the average of both values for the adjacent connections. Finally, the elastic widths for the test structure were determined by reducing the elastic widths for the prototype by half. The effective beam widths with stiffness reductions were computed by multiplying the elastic widths for the test structure by the factor obtained from Eq. (13). To calculate the precise stiffness reduction factor in

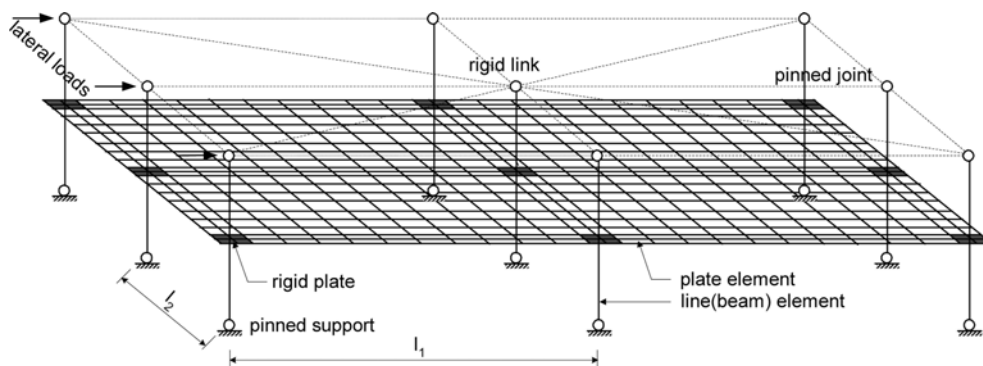


Fig. 15 Finite element model of the test structure

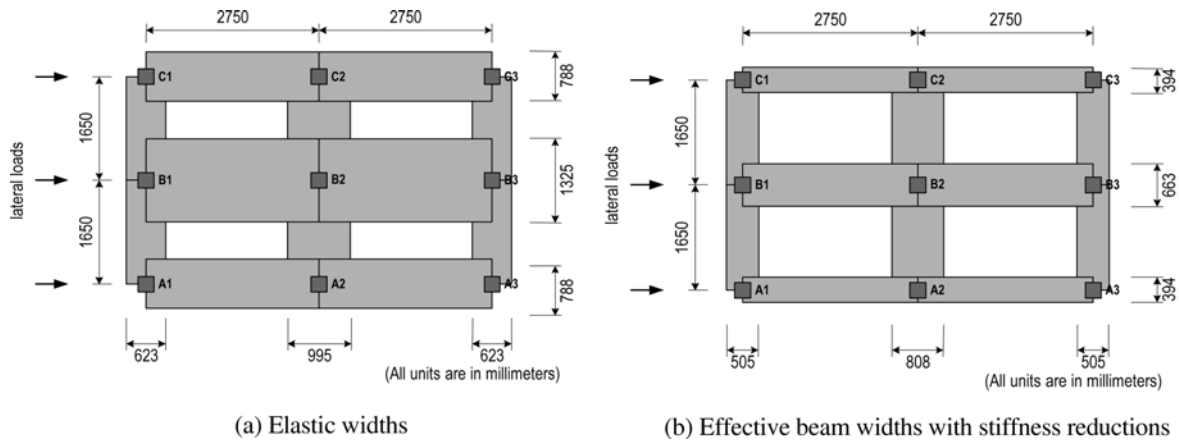


Fig. 16 Comparison of beam element widths in analysis model

Eq. (13), changes in the loading states according to the test procedure were considered. For example, only half of the self-weight (2.11 kN/m^2) of the prototype concrete slab was input into the sustained load term (L_{SUS}), because the test structure was constructed at half scale, and the other half was added to super-imposed load (L_{SUS}). In conformance with ACI 318-02 (2002), a time-dependent term ξ of 1 was used because the lateral loading in the test was applied at around three months after casting. Fig. 16 shows the calculated widths of the beam elements in the effective beam width models without or with stiffness reductions.

4.3 Comparisons between analytical and experimental results

The comparisons between the analytical and experimental results are shown in Fig. 17. The

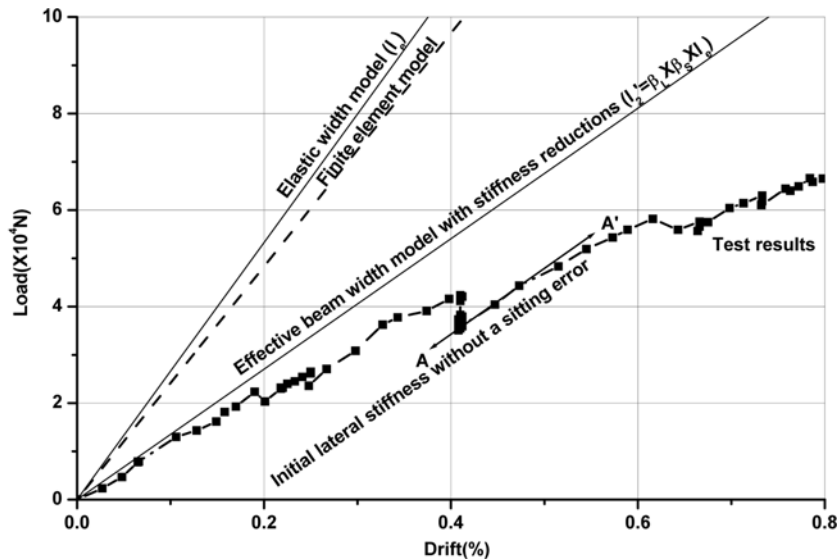


Fig. 17 Comparison of calculated and measured lateral stiffness

experimental results are displayed for up to 0.8 percent of the interstory height for the test structure. The analytical results were obtained by using the finite element model and the effective beam width models. Based on the results of the test and FE analysis, two effective beam width models proposed in this paper were evaluated.

The elastic width model solution slightly exceeds the finite element solution by about 10 percent. This difference may arise since Eqs. (1) and (2) slightly overestimate the elastic stiffness of the slabs within the range of $l_2/l_1 \leq 1$, as discussed previously. Considering that l_2/l_1 of the test structure is equal to 0.6, this difference is predictable. Both the finite element and elastic width model solutions, which do not consider stiffness reductions, are much stiffer than the measured values.

Compared to the elastic width model stiffness, the lateral stiffness of the effective beam width model with stiffness reductions was dramatically reduced as shown in Fig. 17. The solution of the model with effective beam widths of $\beta_L \times \beta_S \times l_e$ conceptually represents the initial lateral stiffness of flat plate structures with vertical loads. The effective beam width model solution with stiffness reductions approximately matches the line A-A'. The line A-A' was obtained after that lateral loading was stopped and applied again at around drifts of 0.4%, and represents the initial value in the lateral stiffness of the test structure without a sitting error.

5. Further research

The results reported in the paper are preliminary and require more numerical studies to confirm them. The numerical studies using three-dimensional non-linear software should focus on the stiffness reductions due to service gravity load, creep and shrinkage, and lateral load.

6. Conclusions

A study to obtain the effective beam widths of slabs was conducted. Based on this study, the following conclusions were reached.

In the elastic widths study using a finite element technique, it was found that the elastic widths were considerably affected by the vertical member's rectangularity, which has usually been ignored for the slab-column connection problem. Based on the results of a parametric study for c_1/l_1 , l_2/l_1 , c_2/c_1 , and c_2/l , the methods for calculating the elastic widths of slabs connected to vertical members with various rectangular cross-sections were proposed.

In the stiffness reduction factors study, the factor (β_S) for service gravity loads was proposed by using the effective moment of inertia (I_e). This value decreased with the increasing of l_n and L_{SUP} , and with the decreasing of f_{ck} and h/h_{min} . The use of the factor (β_L) to consider the combined effects of creep and shrinkage was suggested by modifying the additional long-term deflections (δ_{CP+SH}).

A test structure with nine slab-column connections was tested laterally and analyzed by using a finite element technique. Based on the analytical and experimental results, it was found that the stiffness reduction factors proposed in this study may be used to approximately represent the flexural stiffness of the slab.

Acknowledgements

This study was financially supported by Chonnam National University in program, Post-Doc 2003 and Regional Research Centers Program of the Korean Ministry of Education & Human Resources Development, 2005. The authors wish to thank Scott D.B. Alexander for his advice in revising the paper.

References

- Aalami, B. (1972), "Moment-rotation relation between column and slab", *ACI J.*, **69**(5), 263-269.
- ACI (2002), *Building Code Requirements for Structural Concrete (ACI 318-02) and Commentary (ACI 318R-02)*, American Concrete Institute.
- Allen, F.H. and Darvall, P.L. (1977), "Lateral load equivalent frame", *ACI J.*, **74**(7), 294-299.
- Grossman, J.S. (1997), "Verification of proposed design methodologies for effective width of slabs in slab-column frames", *ACI Struct. J.*, **94**(2), 181-196.
- Hwang, S.J. and Moehle, J.P. (1993), "An experimental study of flat-plate structures under vertical and lateral loads", Report No. UCB/EERC-93/03, Earthquake Engineering Research Center, University of California, Berkeley.
- Hwang, S.J. and Moehle, J.P. (2000), "Models for laterally loaded slab-column frames", *ACI Struct. J.*, **97**(2), 345-352.
- Hwang, S.J. and Moehle, J.P. (2000), "Vertical and lateral load tests of nine-panel flat-plate frame", *ACI Struct. J.*, **97**(1), 193-203.
- MIDAS/Gen Release 5.7.1 (2003), MIDAS Information Technology Co., Ltd., Seoul, Korea.
- Moehle, J.P. and Diebold, J.W. (1984), "Experimental study of the seismic response of a two story flat plate structure", Report No. UCB/EERC-84/08, Earthquake Engineering Research Center, University of California, Berkeley.
- Pan, A.P. and Moehle, J.P. (1992), "An experimental study of slab-column connections", *ACI Struct. J.*, **89**(6), 626-638.
- Patrick, M.D. and Huo, X.S. (2004), "Finite element modeling of slab-on-beam concrete bridge superstructures", *Computers and Concrete, An Int. J.*, **1**(3), 355-369.
- Pecknold, D.A. (1975), "Slab effective width for equivalent frame analysis", *ACI J.*, **72**(4), 135-137.
- Robertson, L.N. and Durrani, A.J. (1992), "Gravity load effect on seismic behavior of interior slab-column connections", *ACI Struct. J.*, **89**(1), 37-45.
- Robertson, L.N. and Durrani, A.J. (1991), "Gravity load effect on seismic behavior of exterior slab-column connections", *ACI Struct. J.*, **88**(3), 255-267.
- Yun, Y.M. (2005), "Strut-tie model evaluation of behavior of strength of pre-tensioned concrete deep beams", *Computers and Concrete, An Int. J.*, **2**(4), 267-291.

Notation

- c_1 : size of rectangular support parallel to loading directions
 c_2 : size of rectangular support transverse to c_1
 DL : service dead load
 EI_{FL} : final flexural stiffness of member at the stage when final deflection (δ_{FL}) is computed
 EI_{DL+LL} : flexural stiffness of member at the stage when immediate deflection (δ_{DL+LL}) is computed
 LL : service live load
 f_{ck} : compressive strength of concrete
 h : thickness of slab

h_{\min}	: minimum thickness of slab (see ACI 318-02 section 9.5.3.2)
I_{cr}	: moment of inertia of the cracked concrete section
I_e	: effective moment of inertia
I_g	: moment of inertia of the gross concrete section
l_1	: length of span parallel to loading directions (average of two spans at interior supports)
l_2	: length of span transverse to loading directions (average of two spans at interior supports)
l_2'	: effective beam width with stiffness reductions
l_e	: elastic effective beam width
l_n	: length of clear span parallel to loading directions
L_{SUP}	: super-imposed load (sum of floor finishing load and live load)
L_{SUS}	: sustained load (sum of dead load and portion of live load)
M_a	: maximum service moment due to gravity load
M_{cr}	: cracking moment (see ACI 318-02 section 9.5.2.3)
β_L	: factor considering stiffness reduction of slabs due to the combined effects of creep and shrinkage
β_S	: factor considering stiffness reduction of slabs due to the effect of service gravity loads
θ_s	: slab rotations at the center of the joint region
θ_{br}	: beam rotations at the end of the beam element with rigid bar
θ_{bf}	: beam rotations at the end of the beam element without rigid bar
δ_{CP+SH}	: additional long-term deflection due to the combined effects of creep and shrinkage
δ_{DL+LL}	: immediate deflection caused by service dead plus live loads
δ_{SUS}	: immediate deflection caused by sustained load
δ_{FL}	: final deflection calculated as the sum of immediate and additional long-term deflections
ξ	: time-dependent factor for sustained load (see ACI 318-02 section 9.5.2.5)
ρ'	: compression reinforcement ratio